Copy /
RM SL9G21a

NACA

RESEARCH MEMORANDUM

for the

Bureau of Aeronautics, Department of the Navy

HIGH-SPEED WIND-TUNNEL INVESTIGATION OF THE LATERAL STABILITY CHARACTERISTICS OF A 0.10-SCALE MODEL OF THE GRUMMAN XF9F-2 AIRPLANE - TED NO. NACA DE 301

By

Edward C. Polhamus and Thomas J. King, Jr.

Langley Aeronautical Laboratory
Langley Air Force Base, Va.

NATIONAL ADVISORY COMMITTEE
FOR AERONAUTICS

WASHINGTON

NATIONAL ADVISORY COMMITTEE FOR AERONAUTICS

RESEARCH MEMORANDUM

for the

Bureau of Aeronautics, Department of the Navy

HIGH-SPEED WIND-TUNNEL INVESTIGATION OF THE LATERAL STABILITY CHARACTERISTICS OF A 0.10-SCALE MODEL OF THE GRUMMAN XF9F-2 AIRPLANE - TED NO. NACA DE 301

By Edward C. Polhamus and Thomas J. King, Jr.

SUMMARY

An investigation was made in the Langley high-speed 7- by 10-foot tunnel to determine the high-speed lateral and directional stability characteristics of a 0.10-scale model of the Grumman XF9F-2 airplane in the Mach number range from 0.40 to 0.85.

The results indicate that static lateral and directional stability is present throughout the Mach number range investigated although in the Mach number range from 0.75 to 0.85 there is an appreciable decrease in rolling moment due to sideslip. Calculations of the dynamic stability indicate that according to current flying-quality requirements the damping of the lateral oscillation, although probably satisfactory for the sea-level condition, may not be satisfactory for the majority of the altitude conditions investigated.

INTRODUCTION

At the request of the Bureau of Aeronautics an investigation of the high-speed stability and control characteristics of a 0.10-scale model of the Grumman XF9F-2 airplane was conducted in the Langley high-speed 7- by 10-foot tunnel.

The results of the longitudinal stability and control investigation have been reported in reference 1. The present paper presents the results of the lateral and directional stability investigation at Mach numbers ranging from 0.40 to 0.85, and includes calculations of the estimated period and damping characteristics of the rudder-fixed lateral oscillation.

COEFFICIENTS AND SYMBOLS

The stability system of axes used for the presentation of the data, together with an indication of the positive forces, moments, and angles, is presented in figure 1. The symbols used are defined as follows:

C_L	lift coefficient (Lift/qS)
C_l	rolling-moment coefficient (L/qSb)
C_n	yawing-moment coefficient (N/qSb)
C_Y	lateral-force coefficient (Y/qS)
L	rolling moment, foot-pounds
N	yawing moment, foot-pounds
Y	lateral force, pounds
W	weight, pounds
q	free-stream dynamic pressure, pounds per square foot ($\rho V^2/2$)
ρ	mass density of air, slugs per cubic foot
V	free-stream velocity, feet per second
S	wing area, square feet
b	wing span, feet
M	Mach number (V/a)
a	velocity of sound, feet per second

R	Reynolds number $(\rho V c'/\mu)$
μ	absolute viscosity of air, slugs per foot–second
α	angle of attack of model, measured from the X–axis to the fuselage reference line, degrees
β	angle of sideslip, radians
ψ	angle of yaw, degrees
η	angle of attack of principal longitudinal axis of airplane, positive when principal axis is above flight path at the nose, degrees
ϵ	angle between fuselage reference line and principal axis, positive when fuselage reference line is above principal axis, degrees
γ	angle of flight path to horizontal axis, positive in a climb, degrees
P	rolling angular velocity, radians per second
r	yawing angular velocity, radians per second
k_X	radius of gyration in roll about principal longitudinal axis, feet
k_Z	radius of gyration about principal normal axis, feet
P	period, seconds
$C_{1/2}$	cycles to damp to one–half amplitude
$T_{1/2}$	time to damp to one–half amplitude, seconds

$$C_{l_\psi} = \frac{\partial C_l}{\partial \psi}$$

$$C_{n_\psi} = \frac{\partial C_n}{\partial \psi}$$

$$C_{Y_\psi} = \frac{\partial C_Y}{\partial \psi}$$

$$C_{l_p} = \frac{\partial C_l}{\partial \frac{pb}{2V}}$$

$$C_{n_p} = \frac{\partial C_n}{\partial \frac{pb}{2V}}$$

$$C_{l_r} = \frac{\partial C_l}{\partial \frac{rb}{2V}}$$

$$C_{n_r} = \frac{\partial C_n}{\partial \frac{rb}{2V}}$$

APPARATUS AND METHODS

Tunnel and Model

The tests were conducted in the Langley high-speed 7- by 10-foot tunnel, which is a closed rectangular tunnel of the return-flow type with a contraction ratio of 15.7 to 1.

The 0.10-scale steel model was constructed at the David Taylor Model Basin, Carderock, Maryland. Details of the model as tested are presented in figure 2. The model was tested through a Mach number range of 0.40 to 0.85 at various angles of yaw on the sting support shown in figure 3.

The variation of test Reynolds number with Mach number for average test conditions is presented in figure 4. The degree of turbulence of the tunnel is not known but is believed to be small because of the high contraction ratio. Experience has indicated that for a model of this size constriction effects should not invalidate the test results at corrected Mach numbers below about 0.91.

Support System

A sting-support system was used to support the model in the tunnel and a photograph of the test setup is presented as figure 3. The sting extended from the rear of the fuselage to a vertical strut located

behind the test section. This strut was mounted on the tunnel balance system and was shielded from the air stream by a streamline fairing. The tare forces and moments produced by the sting were determined through the Mach number range by mounting the model on two wing stings, which were also attached to the vertical strut, and testing the model with and without the center sting. With the center sting in place, the duct flow was bypassed through a hole in the underside of the aft portion of the fuselage, while without the center sting, the flow was exhausted out of the rear of the fuselage. Therefore, the corrected data represent, within practical limits, the power-off condition with flow out of the rear of the fuselage. Angles of yaw were changed by the use of interchangeable couplings in the stings aft of the model. The deflections of the support system under load were determined from static loading tests.

Corrections

The test results have been corrected for the tare forces and moments produced by the support system. The corrections due to the jet-boundary induced upwash were computed and found to be negligible and therefore have not been applied. The dynamic pressure and Mach number have been corrected for blocking by the model and its wake by the method of reference 2.

DISCUSSION

Basic data.- The basic data are presented in figure 5 in the form of side-force, yawing-moment, and rolling-moment coefficients plotted against angle of yaw at zero angle of attack for various Mach numbers from 0.40 to 0.85.

Lateral-stability parameters.- The lateral-stability parameters, obtained from the basic data of figure 5, are presented as a function of Mach number in figure 6. The values, when extrapolated to a Mach number of 0.18, are in good agreement with the low-speed wind-tunnel results presented in reference 3 with the exception of the effective dihedral parameter C_{l_ψ} which appears to be about 15 percent higher than the low-speed value. However, the low-speed model was tested without tip tanks, and it has been demonstrated on similar models (for example, fig. 29 of reference 4) that tip tanks can easily increase the dihedral effect by this amount.

At a Mach number of 0.40 the effective dihedral parameter C_{l_ψ} is equivalent to about 10° of positive geometric dihedral and increases with Mach number up to 0.75 where it is equivalent to about 15° of positive geometric dihedral. (See reference 5.) Above a Mach number

of 0.75 there is a decrease in the effective dihedral with increasing Mach number which is probably due to a loss in the wing dihedral effect since the loss occurs at the same Mach number as the loss in lift-curve slope. (See fig. 10 of reference 1.)

Static directional stability C_{n_ψ} is present throughout the Mach number range and increases from a value of −0.0021 at a Mach number of 0.40 to a value of −0.0027 at a Mach number of 0.85.

Dynamic stability.- The period of the rudder-fixed lateral oscillation and the time and cycles required to damp the oscillation to one-half amplitude have been evaluated by the method of reference 6 and are presented in figure 7 for several wing loadings and altitudes throughout the Mach number range. The various parameters used in the calculations are presented in table I. The rotary derivatives were estimated with the aid of references 3 and 7 to 10. Also, presented in figure 7 is a comparison of the damping characteristics with the requirements set forth in reference 11. According to these requirements, the damping of the oscillation is satisfactory for the sea-level condition but unsatisfactory for the majority of the altitude conditions investigated.

CONCLUSIONS

Based on high-speed wind-tunnel tests of the lateral stability characteristics of a 0.10-scale model of the Grumman XF9F-2 airplane in the Mach number range from 0.40 to 0.85, the following conclusions have been drawn:

1. Static lateral and directional stability is present throughout the Mach number range investigated although in the Mach number range from 0.75 to 0.85 there is an appreciable decrease in rolling moment due to sideslip.

2. Calculations of the dynamic stability indicate that according to current flying-quality requirements the damping of the lateral oscillation, although probably satisfactory for the sea-level condition, may not be satisfactory for the majority of the altitude conditions investigated.

Langley Aeronautical Laboratory
National Advisory Committee for Aeronautics
Langley Air Force Base, Va.

Edward C. Polhamus
Edward C. Polhamus
Aeronautical Research Scientist

Edward C. Polhamus
for Thomas J. King, Jr.
Aeronautical Research Scientist

Approved:

Thomas A. Harris
Thomas A. Harris
Chief of Stability Research Division

rw

REFERENCES

1. Polhamus, Edward C., and King, Thomas J., Jr.: High-Speed Wind-Tunnel Investigation of the Longitudinal Stability and Control Characteristics of a 0.10-Scale Model of the Grumman XF9F-2 Airplane - TED No. NACA DE 301. NACA RM SL8K16, Bur. Aero., 1948.

2. Herriot, John G.: Blockage Corrections for Three-Dimensional-Flow Closed-Throat Wind Tunnels, with Consideration of the Effect of Compressibility. NACA RM A7B28, 1947.

3. Tamburello, V., and Beek, Charles R.: Wind-Tunnel Tests of a 1/5-Scale Powered Model of the XF9F-2 Airplane. Part VII - Lateral Stability and Control - TED No. TMB DE 301. The David W. Taylor Model Basin, Navy Dept., Rep. C-215, Aero 758, April 1949.

4. Tucker, Warren A., and Goodson, Kenneth W.: Tests of a 1/5-Scale Model of the Republic XP-84 Airplane (Army Project MX-578) in the Langley 300 MPH 7- by 10-Foot Tunnel. NACA MR L6F25, Army Air Forces, 1946.

5. Luckert, H. J.: Lift Distribution on Wings with Dihedral in Yaw. Reps. and Translations No. 742, British M.O.S.(A) Völkenrode, May 1947.

6. Sternfield, Leonard: Some Considerations of the Lateral Stability of High-Speed Aircraft. NACA TN 1282, 1947.

7. Toll, Thomas A., and Queijo, M. J.: Approximate Relations and Charts for Low-Speed Stability Derivatives of Swept Wings. NACA TN 1581, 1948.

8. Bird, John D.: Some Theoretical Low-Speed Span Loading Characteristics of Swept Wings in Roll and Sideslip. NACA TN 1839, 1949.

9. Fisher, Lewis R.: Approximate Corrections for the Effects of Compressibility on the Subsonic Stability Derivatives of Swept Wings. NACA TN 1854, 1949.

10. Murray, Harry E. and Wells, Evalyn G.: Wind-Tunnel Investigation of the Effect of Wing-Tip Fuel Tanks on Characteristics of Unswept Wings in Steady Roll. NACA TN 1317, 1947.

11. Anon.: Specification for Flying Qualities of Piloted Airplanes. NAVAER SR-119B, Bur. Aero., June 1, 1948.

TABLE I

PARAMETERS USED IN THE CALCULATIONS OF THE PERIODS AND DAMPING

OF THE LATERAL OSCILLATION OF THE GRUMMAN XF9F-2 AIRPLANE

W/S	Altitude	M	k_X^2	k_Z^2	ϵ	η	γ	C_L	C_{l_p}	C_{l_r}	C_{n_p}	C_{n_r}	C_{l_β}	C_{n_β}	C_{Y_β}
60	30,000	0.60	40.50	79.80	2.8	1.4	0	0.379	−0.544	0.147	0.027	−0.231	−0.114	0.129	−0.631
		.70				0		.279	−.546	.132	.038	−.230	−.119	.135	−.671
		.75				−.6		.243	−.571	.128	.042	−.229	−.122	.140	−.688
		.80				−.6		.213	−.584	.126	.043	−.232	−.109	.146	−.711
		.85				−.4		.190	−.594	.122	.041	−.246	−.056	.155	−.718
60	Sea level	0.40	40.50	79.80	2.8	0.3	0	0.253	−0.519	0.110	0.036	−0.229	−0.110	0.120	−0.619
		.60				−1.3		.112	−.544	.084	.049	−.228	−.114	.129	−.639
		.70				−1.8		.083	−.546	.080	.052	−.228	−.119	.135	−.671
		.75				−1.9		.072	−.571	.079	.053	−.227	−.122	.140	−.688
		.80				−1.9		.063	−.584	.078	.054	−.231	−.109	.146	−.711
		.85				−1.8		.056	−.594	.078	.054	−.245	−.056	.155	−.718
40	30,000	0.40	13.75	66.80	2.8	3.8	0	0.569	−0.519	0.173	0.008	−0.236	−0.110	0.120	−0.619
		.60				0		.253	−.544	.118	.038	−.229	−.114	.129	−.631
		.70				−.9		.186	−.546	.107	.045	−.228	−.119	.135	−.671
		.75				−1.3		.162	−.571	.105	.048	−.228	−.122	.140	−.688
		.80				−1.2		.142	−.584	.103	.048	−.231	−.109	.146	−.711
		.85				−.6		.126	−.594	.101	.047	−.245	−.056	.155	−.718
40	Sea level	0.40	13.75	66.80	2.8	−0.6	0	0.169	−0.519	0.092	0.043	−0.228	−0.110	0.120	−0.619
		.60				−1.6		.075	−.544	.075	.052	−.228	−.114	.129	−.631
		.70				−2.0		.055	−.546	.073	.054	−.227	−.119	.135	−.671
		.75				−2.1		.048	−.571	.072	.055	−.227	−.122	.140	−.688
		.80				−2.1		.042	−.584	.072	.055	−.231	−.109	.146	−.711
		.85				−2.1		.037	−.594	.071	.056	−.245	−.056	.155	−.718

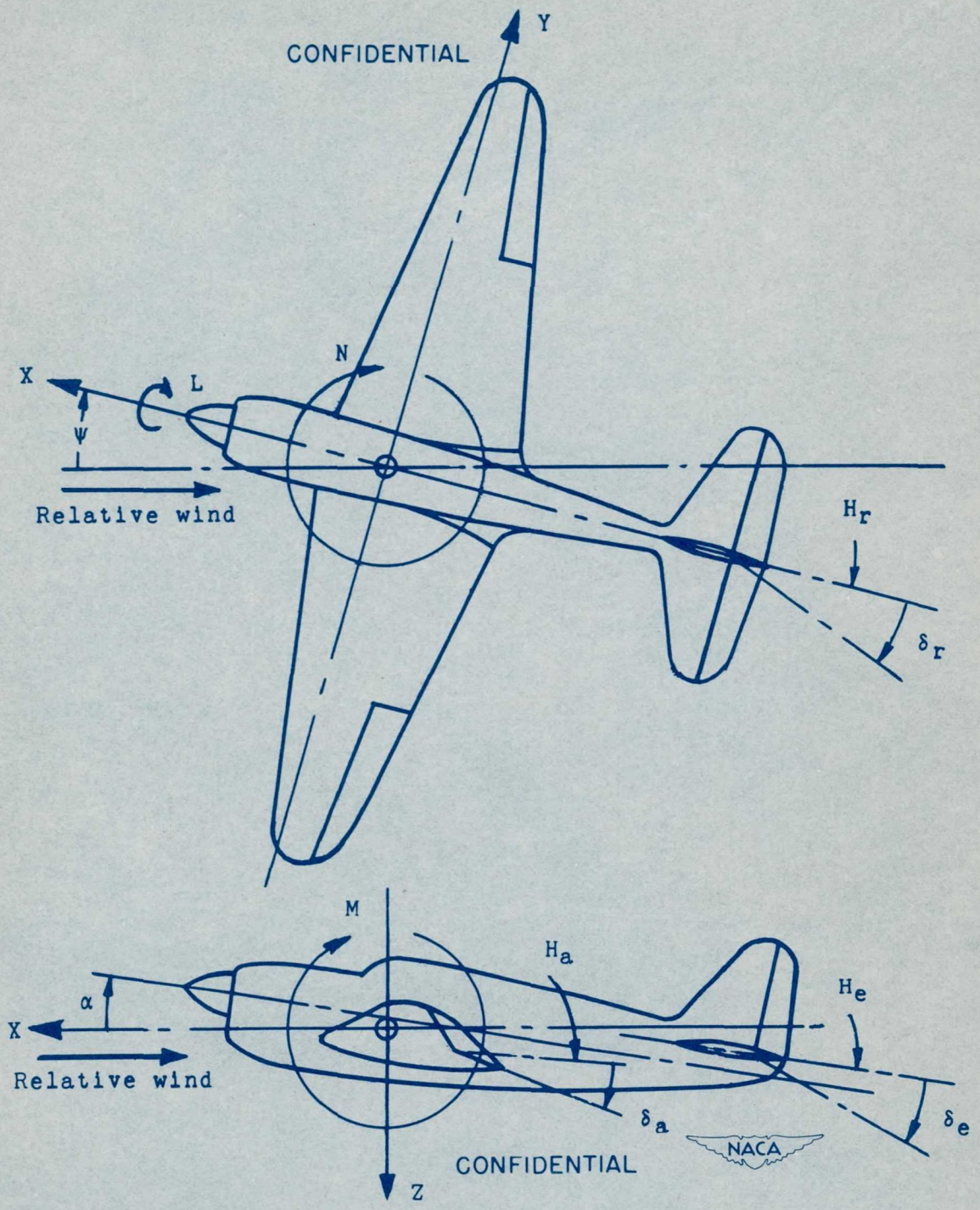

Figure 1.– System of axes and control-surface hinge moments and deflections. Positive values of forces, moments, and angles are indicated by arrows. Positive values of tab hinge moments and deflections are in the same directions as the positive values for the control surfaces to which the tabs are attached.

CONFIDENTIAL

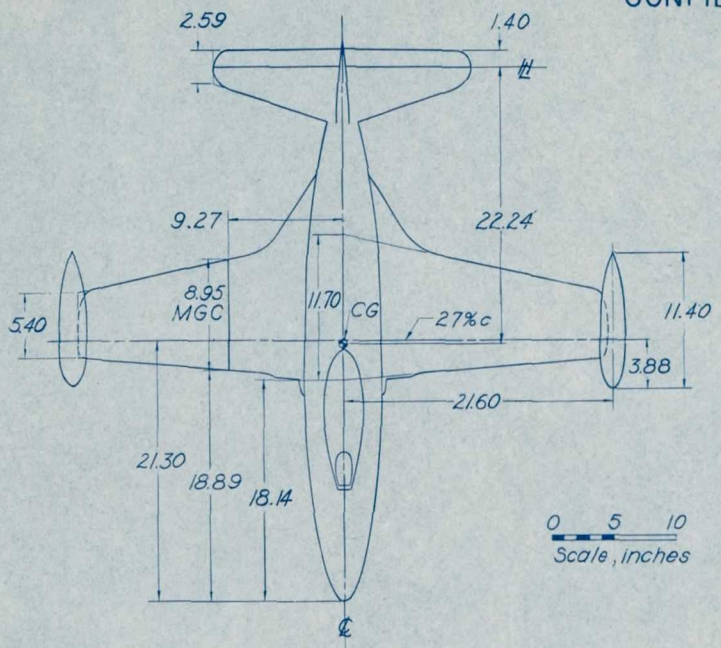

TABULATED DATA

Wing		
Section		NACA 64_1A012
Incidence		0°
Taper ratio		0.46
Aspect ratio		4.97
Area		2.500 sq ft
Mean Geometric Chord		0.746 ft
Horizontal tail		
Section	Tip	NACA 64A010
	Root	NACA 64_1A012
Taper ratio		0.417
Aspect ratio		4.71
Area		0.626 sq ft

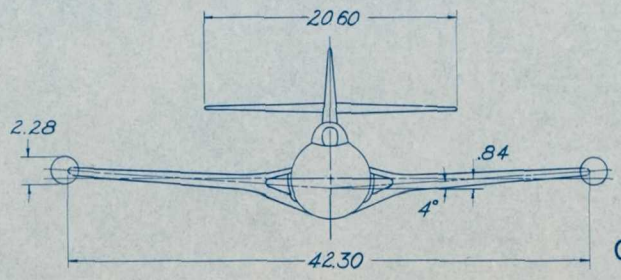

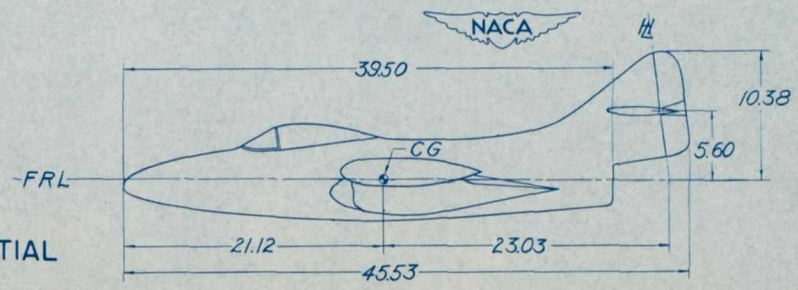

CONFIDENTIAL

Figure 2.- General arrangement of 0.10-scale model of Grumman XF9F-2 airplane.

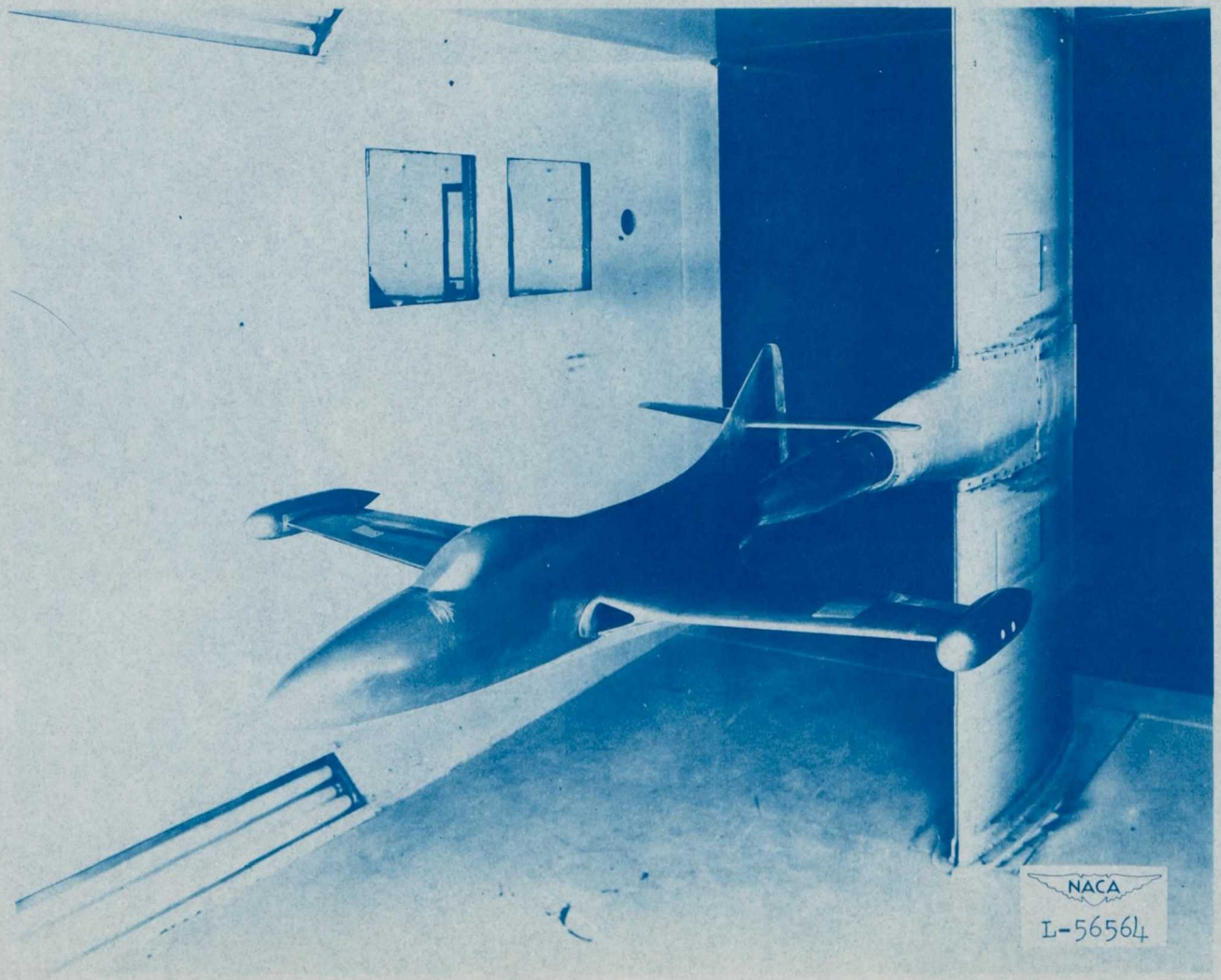

Figure 3.- Photograph of the 0.10-scale model of the Grumman XF9F-2 airplane mounted on the sting support.

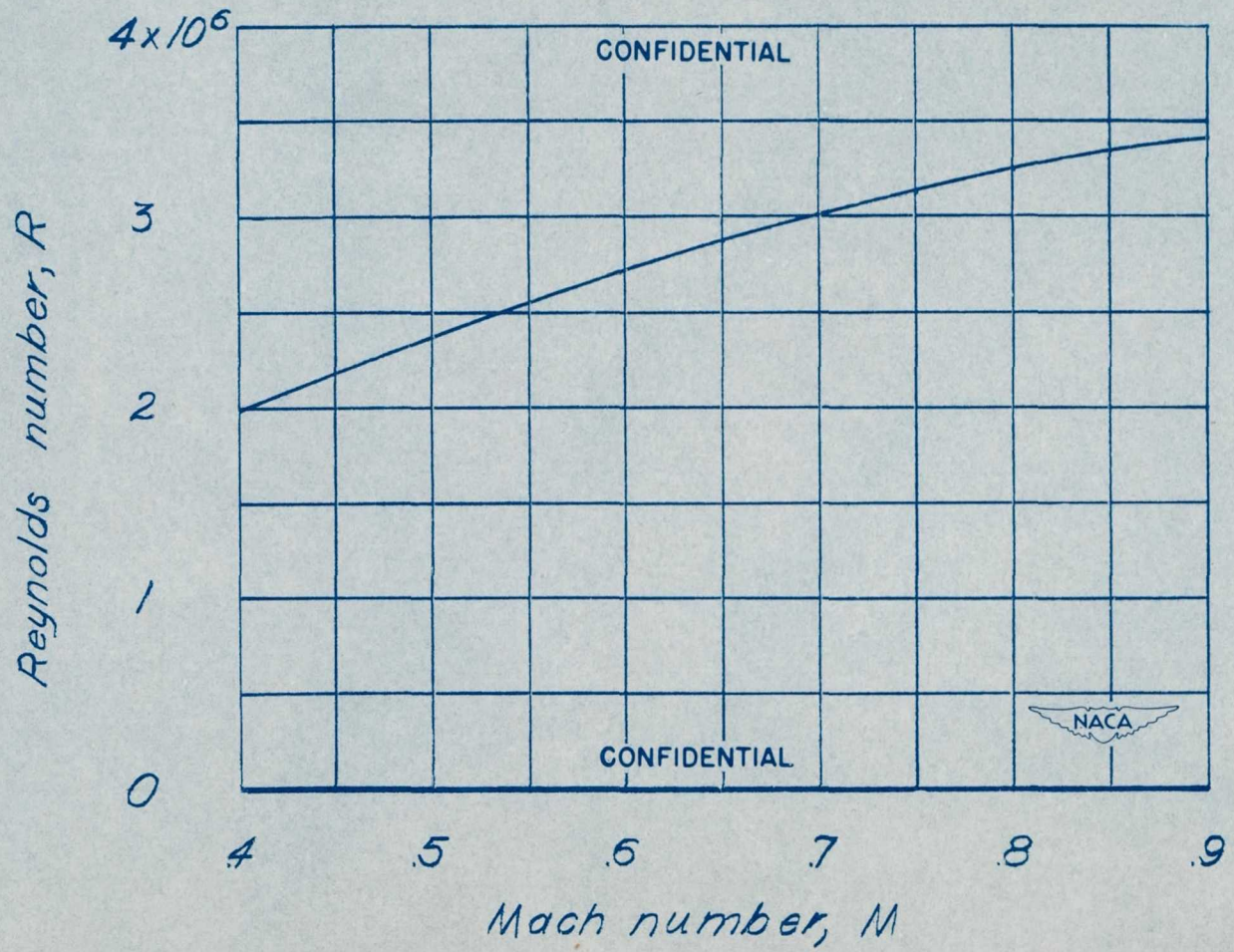

Figure 4.- Variation of test Reynolds number with Mach number for the 0.10-scale model of the Grumman XF9F-2 airplane.

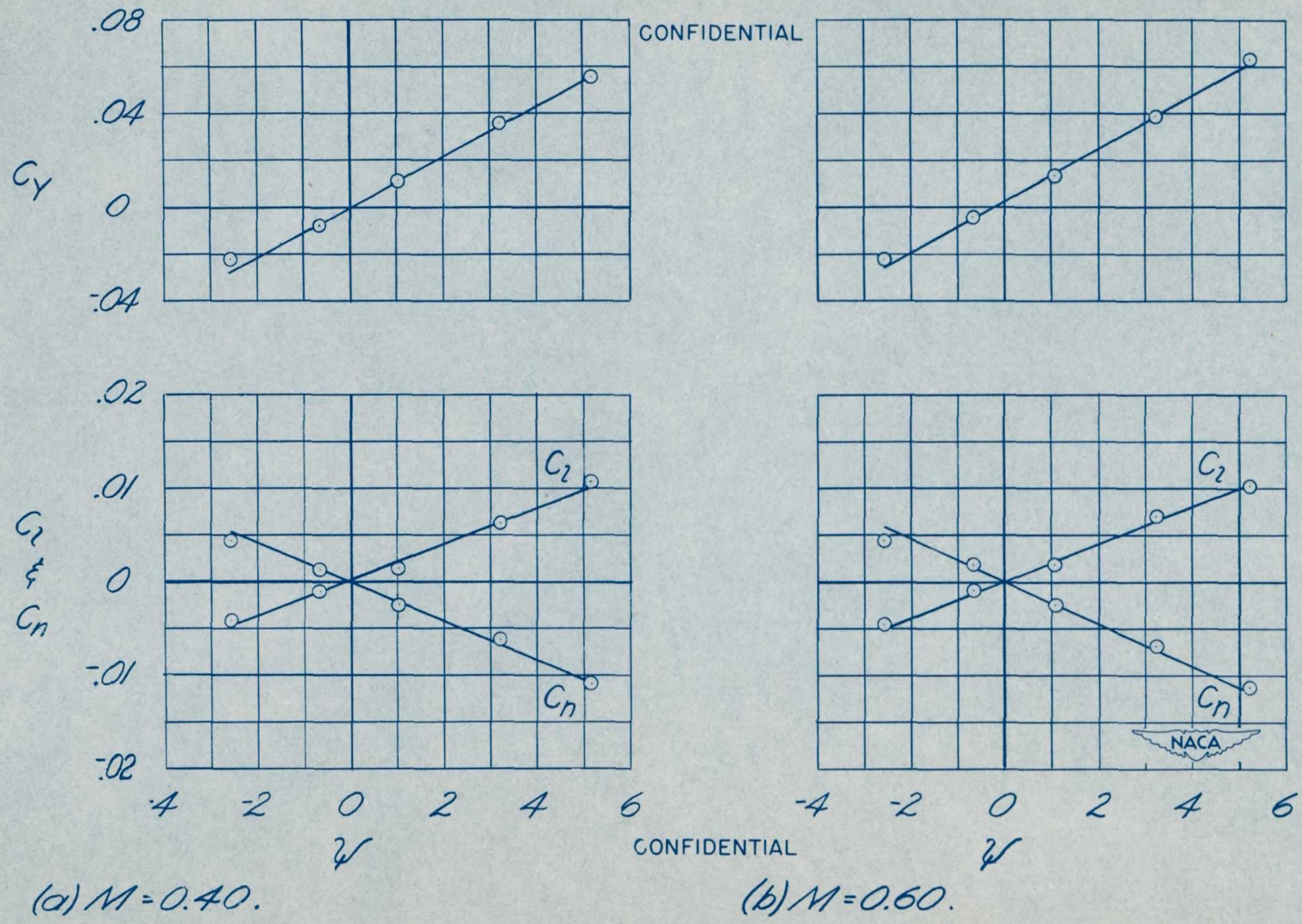

Figure 5.– Aerodynamic characteristics in yaw of the 0.10–scale model of the Grumman XF9F–2 airplane, $\alpha = 0^{\circ}$.

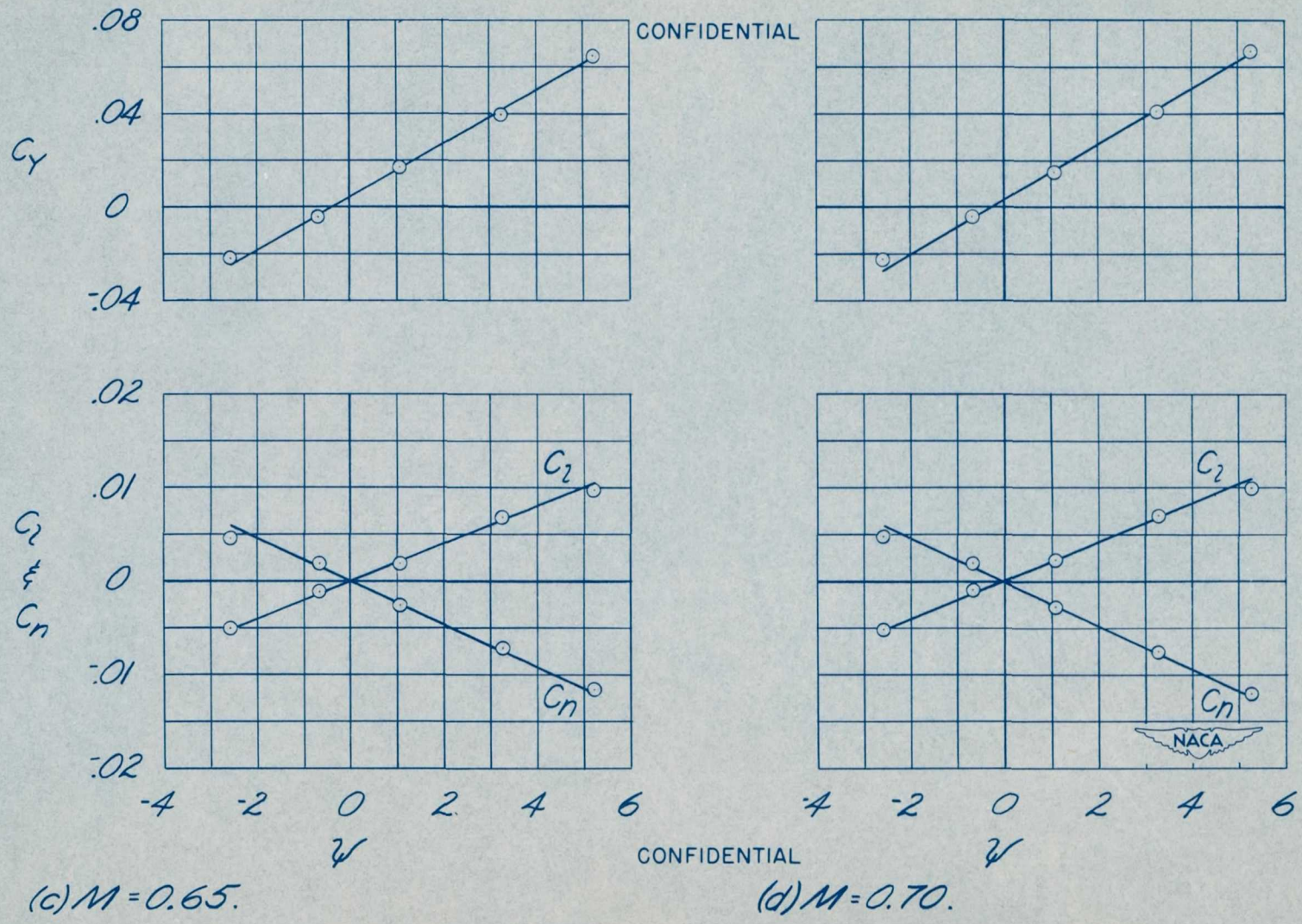

(c) $M = 0.65$.

(d) $M = 0.70$.

Figure 5.– Continued.

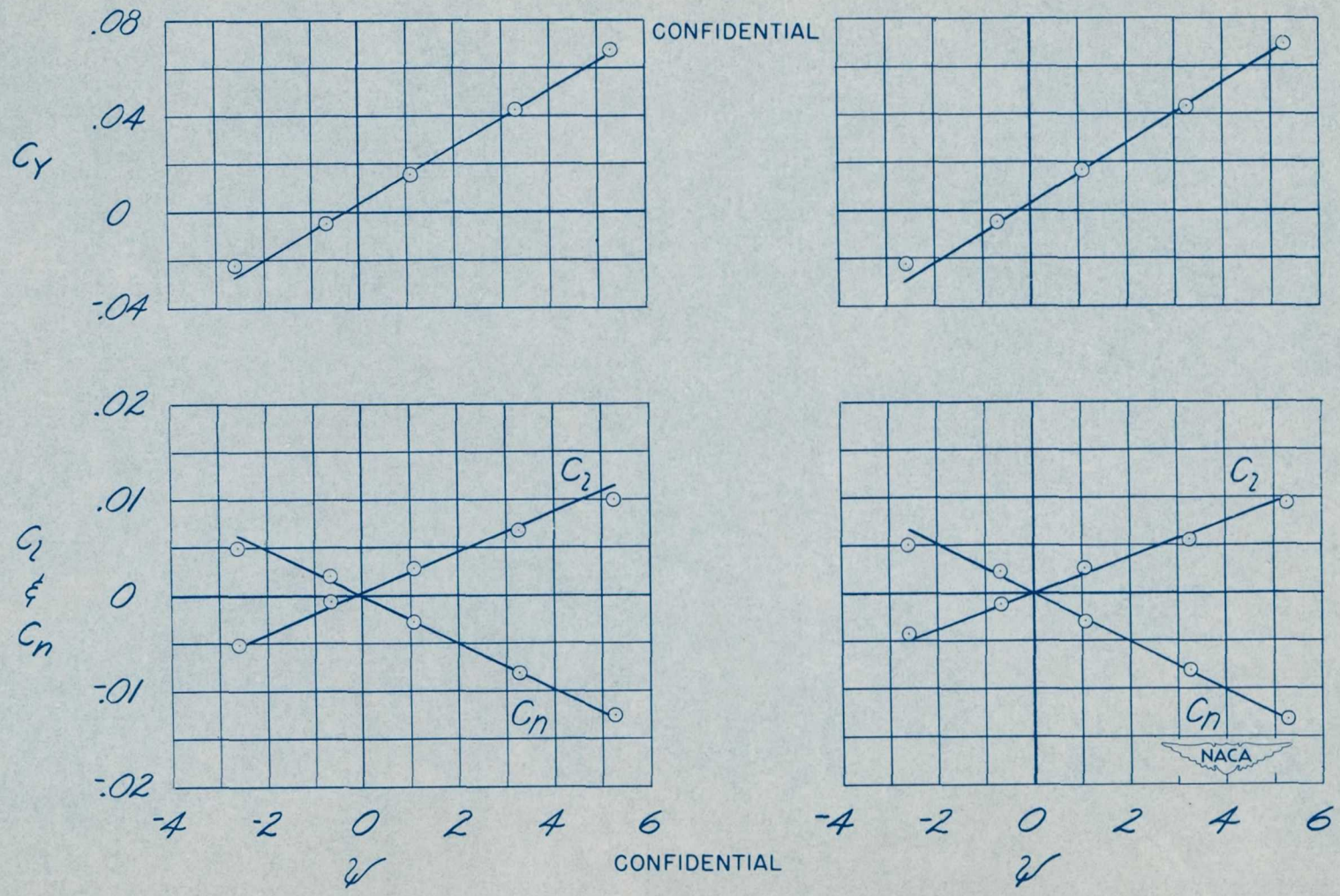

(e) $M = 0.75$.

(f) $M = 0.80$.

Figure 5.– Continued.

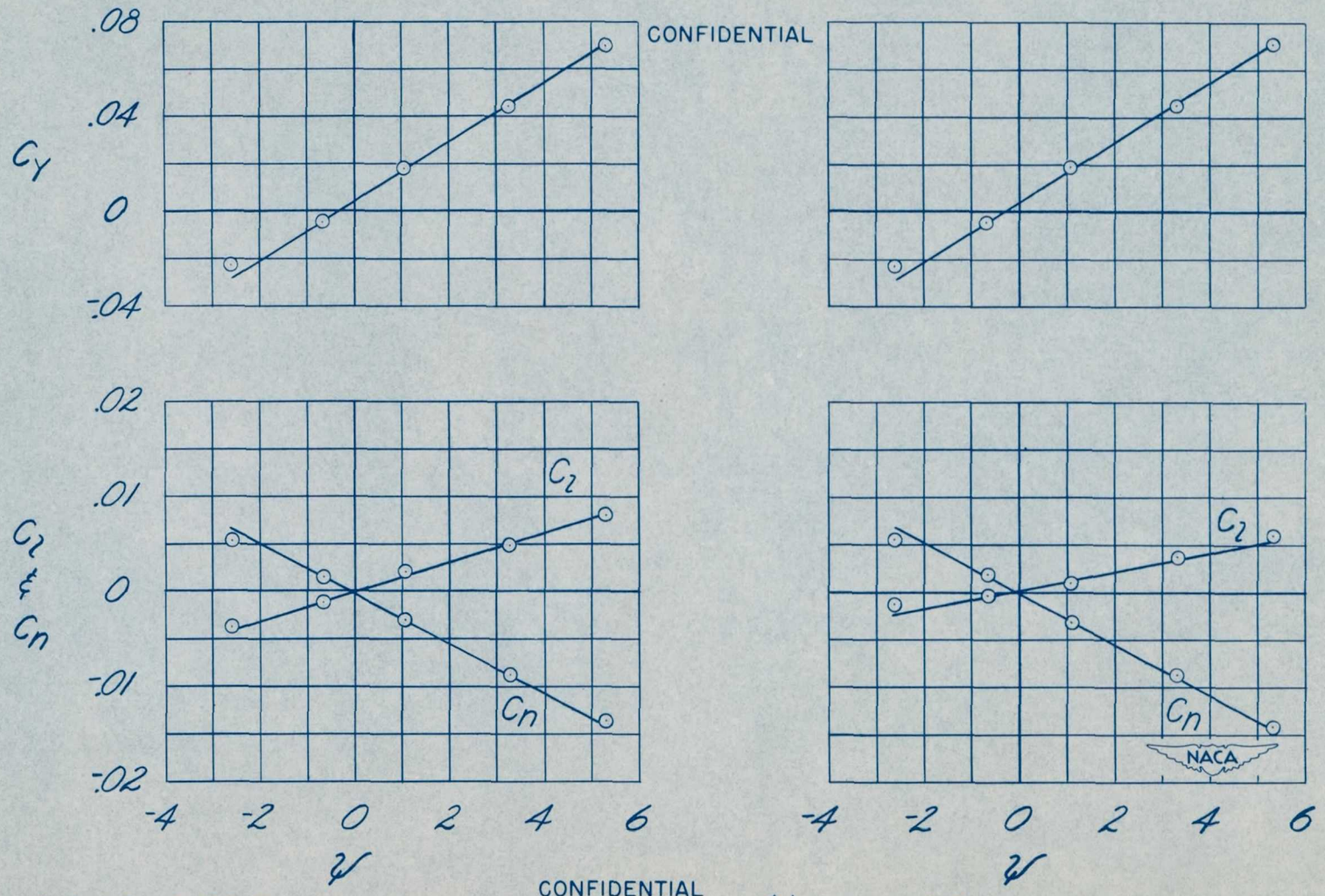

(g) $M = 0.825$.

(h) $M = 0.85$.

Figure 5.- Concluded.

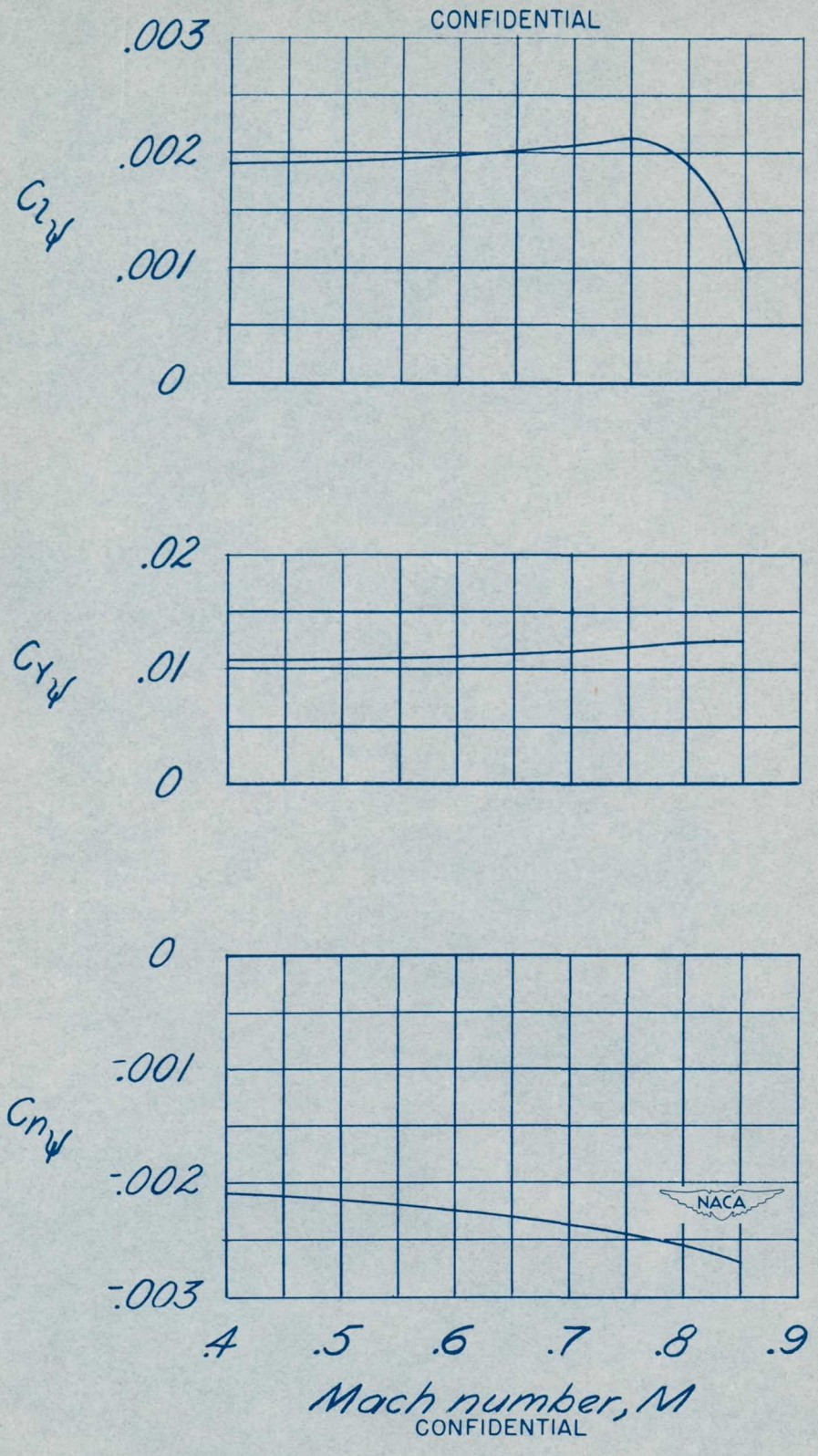

Figure 6.– Effect of Mach number on the lateral–stability parameters of the 0.10–scale model of the Grumman XF9F–2 airplane, $\alpha = 0^{\circ}$.

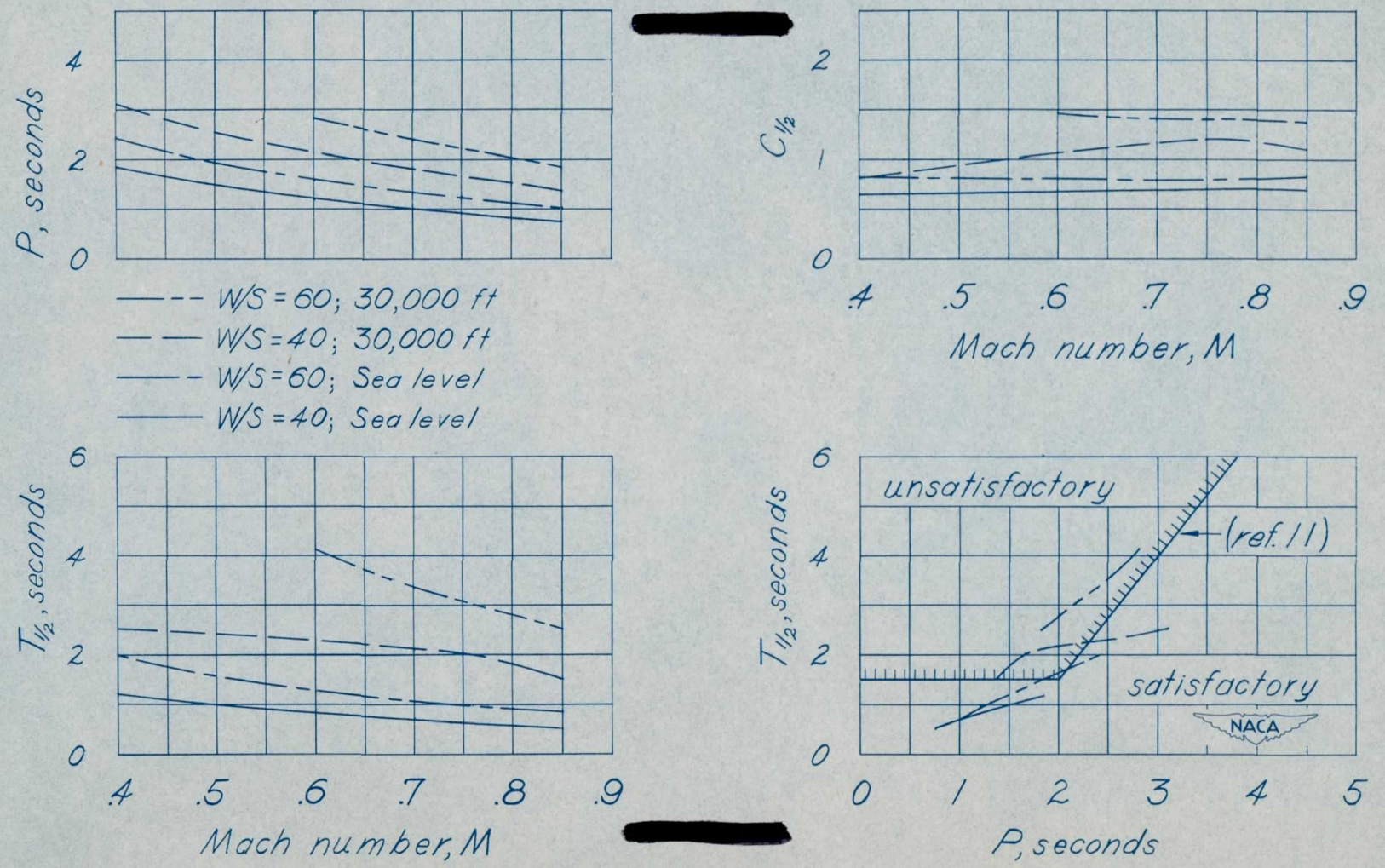

Figure 7.– Estimated characteristics of the lateral oscillation of the Grumman XF9F–2 airplane.